JACS JOURNAL OF THE AMERICAN CHEMICAL SOCIETY

Communication

Cite This: J. Am. Chem. Soc. 2018, 140, 131−134

pubs.acs.org/JACS

^{1}H NMR Spectroscopy of [FeFe] Hydrogenase: Insight into the Electronic Structure of the Active Site

Sigrun Rumpel,*[,†] Enrico Ravera,[‡] Constanze Sommer,[†] Edward Reijerse,[†] Christophe Farès,[§] Claudio Luchinat,[‡] and Wolfgang Lubitz*[,†]

[†]Max-Planck-Institut für Chemische Energiekonversion, Stiftstrasse 34-36, 45470 Mülheim an der Ruhr, Germany

[‡]Department of Chemistry "Ugo Schiff" and Magnetic Resonance Center (CERM), University of Florence and Interuniversity Consortium for Magnetic Resonance of Metallo Proteins (CIRMMP), Via L. Sacconi 6, 50019 Sesto Fiorentino, Italy

[§]Max-Planck-Institut für Kohlenforschung, Kaiser-Wilhelm Platz 1, 45470 Mülheim an der Ruhr, Germany

Supporting Information

ABSTRACT: The [FeFe] hydrogenase HydA1 from *Chlamydomonas reinhardtii* has been studied using ^{1}H NMR spectroscopy identifying the paramagnetically shifted ^{1}H resonances associated with both the $[4Fe\text{-}4S]_H$ and the $[2Fe]_H$ subclusters of the active site "H-cluster". The signal pattern of the unmaturated HydA1 containing only $[4Fe\text{-}4S]_H$ is reminiscent of bacterial-type ferredoxins. The spectra of maturated HydA1, with a complete H-cluster in the active H_{ox} and the CO-inhibited H_{ox}−CO state, reveal additional upfield and downfield shifted ^{1}H resonances originating from the four methylene protons of the azadithiolate ligand in the $[2Fe]_H$ subsite. The two axial protons are affected by positive spin density, while the two equatorial protons experience negative spin density. These protons can be used as important probes sensing the effects of ligand-binding to the catalytic site of the H-cluster.

Hydrogenases are metalloenzymes that catalyze the reversible conversion of dihydrogen into protons and electrons with the class of [FeFe] hydrogenases being the most active hydrogen producers.[1] The unique [6Fe] active site of these enzymes, the so-called "H-cluster", serves as inspiration for the development of inorganic catalysts for production of solar fuels or as part of fuel cells. The H-cluster consists of a $[4Fe\text{-}4S]_H$ cluster connected to the protein via four cysteines, one of which bridges to a unique binuclear Fe subsite $[2Fe]_H$ containing a proximal (Fe_p) and a distal iron (Fe_d) (Figure 1). In contrast to most [FeFe] hydrogenases, HydA1 from *Chlamydomonas reinhardtii* with a molecular weight of about 48 kDa contains no accessory iron sulfur clusters and is thus particularly well suited for spectroscopic investigations of structure and function of the H-cluster. Large quantities of fully active HydA1 can be prepared by the addition of the synthesized inorganic cofactor precursor $[Fe_2(adt)(CO)_4(CN)_2]$ (adt = azadithiolate) to recombinant HydA1 containing only the $[4Fe\text{-}4S]_H$ cluster (apo-HydA1) (Figure 1).[2,3] The active site and its highly conserved protein environment are suggested to act synergistically for efficient hydrogen evolution. The electronic structure of the different redox states of the H-cluster has been well characterized by

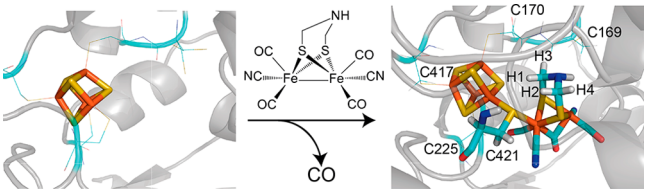

Figure 1. Maturation of HydA1 containing only the $[4Fe\text{-}4S]_H$ cluster with the synthetic precursor $[Fe_2(adt)(CO)_4(CN)_2]$ of the binuclear Fe subsite results in fully functional HydA1. The images of the $[4Fe\text{-}4S]_H$ cluster and the H-cluster are based on PDB entries 3LX4 and 3C8Y, respectively. The metal clusters and the bridging cysteine are shown as sticks with the following color coding; iron, orange; sulfur, yellow; carbon, cyan; oxygen, red; nitrogen, blue.

EPR and FTIR spectroscopy.[4−9] Electronic coupling between the $[4Fe\text{-}4S]_H$ and $[2Fe]_H$ subclusters is of central importance to the electron flow during catalysis.[10] The intimate contact between $[4Fe\text{-}4S]_H$ and $[2Fe]_H$ sites translates into magnetic exchange coupling, which has been demonstrated at low temperatures by Mössbauer and EPR/ENDOR spectroscopy.[11,12] However, the spin density distribution over the H-cluster and the influence of the protein environment have never been studied in solution at room temperature. Here, the method of choice is solution NMR spectroscopy, which can reveal sign and magnitude of the spin density at each NMR active nucleus. Protons are the most sensitive ones, although other magnetic nuclei, e.g., ^{13}C and ^{15}N, could also be studied easily by NMR techniques.[13] For hydrogenases, protons are of particular importance since they are substrate and product of the reversible enzymatic reaction. In principle, NMR allows one in a unique way to directly follow the hydrogen species during the catalytic cycle under physiological conditions.

Here, we present the first NMR spectroscopic investigation of a hydrogenase enzyme, the [FeFe] hydrogenase HydA1. Similar to other iron sulfur proteins, magnetic coupling among iron centers reduces the NMR line widths and renders the spectroscopic investigation feasible.[14] The β-CH_2 protons of the four cysteines coordinating $[4Fe\text{-}4S]_H$ as well as the protons within the $[2Fe]_H$ site are contact shifted out of the diamagnetic envelope (−1 to 11 ppm). Size and sign of the

Received: October 27, 2017
Published: December 6, 2017

DOI: 10.1021/jacs.7b11196
J. Am. Chem. Soc. 2018, 140, 131−134

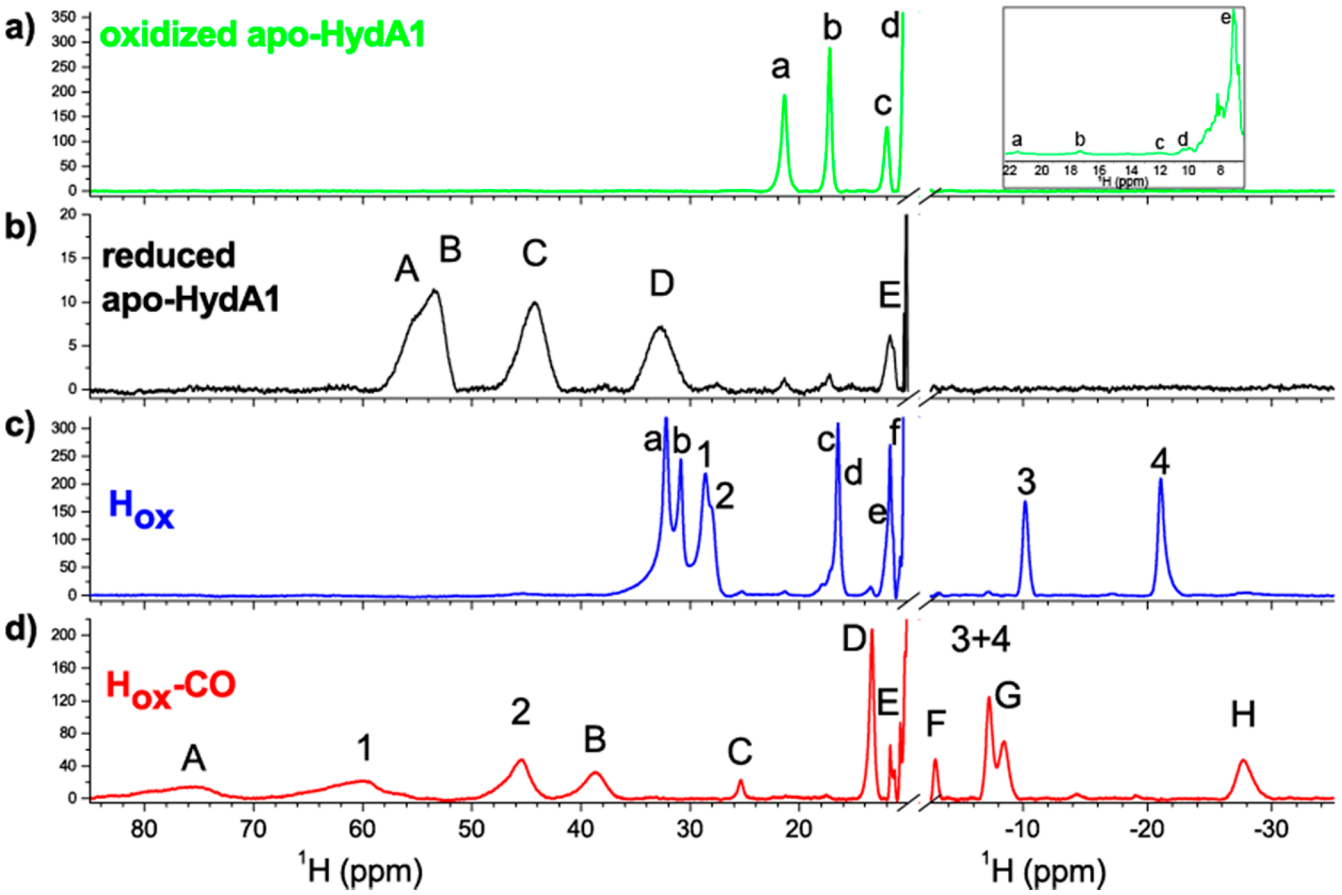

Figure 2. Downfield and upfield region of the 1D ^{1}H NMR spectra (600 MHz) at 298 K of (a) oxidized apo-HydA1 (green line), (b) reduced apo-HydA1 (black line), (c) oxidized HydA1 (blue line, H_{ox}), and (d) CO-inhibited oxidized HydA1 (red line, H_{ox}–CO). Downfield region and upfield region are shown from 85 to 10 ppm and −2.5 to −35 ppm, respectively. Contact shifted cysteine resonances are labeled a–e in (a), A–E in (b), a–f in (c), and A–H in (d). Labels 1, 2, 3, and 4 indicate ^{1}H resonances of $[2Fe]_H$. The inset of (a) shows the spectrum of oxidized apo-HydA1 from 6 to 22 ppm.

contact shift depend on (i) the spin state of the Fe in the cluster to which the cysteine is attached, (ii) the spin density at the nucleus, which largely depends on the Fe–S–Cβ–βCH$_2$ dihedral angle θ, and (iii) temperature.[15] Although the hyperfine shifted signals are significantly broadened due to the interaction of the unpaired electron(s) with the resonating nucleus, they provide a distinctive fingerprint of the cluster environment and protons inherent in the H-cluster. To our knowledge, the only other iron sulfur proteins of high molecular weight studied by NMR are the homodimeric nitrogenase Fe-protein[16] and the hemeprotein subunit of sulfite reductase.[17] The results presented here provide unique insight into structure and function of [FeFe] hydrogenases in solution at room temperature including an exclusive view of the catalytically active H_{ox} state. These data open new prospects to unravel intimate details about geometric and electronic structure of the H-cluster and the influence of the surrounding amino acids.

The amenability of HydA1 to a high-resolution NMR study is demonstrated on oxidized apo-HydA1. The measured ^{1}H NMR spectra reveal three contact shifted resonances downfield of 11 ppm with line width up to 300 Hz (Figure 2a and Table S2). Their pattern resembles bacterial-type ferredoxins in the oxidized $[4Fe\text{-}4S]^{2+}$ form,[18−20] which can be viewed as two antiferromagnetically coupled Fe(II)Fe(III) pairs that form a diamagnetic ground state with a total spin state $S = 0$.[21] Paramagnetism arises at room temperature due to population of low-lying excited states with $S = 1$, 2, etc. Consistent with an oxidized $[4Fe\text{-}4S]^{2+}_H$, all contact shifted resonances exhibit anti-Curie temperature dependence (Table S2 and Figure S1a).[18−20]

Reduction of the $[4Fe\text{-}4S]^{2+}_H$ cluster to the $[4Fe\text{-}4S]^{+}_H$ form is accompanied by about four-fold increased contact shifts and line widths, which is in agreement with a paramagnetic $S = 1/2$ ground state (Figure 2b). For reduced apo-HydA1, the downfield shifted resonances A and D exhibit Curie, whereas B and C show anti-Curie temperature dependence (Figure S1b). Based on their chemical shifts and line widths, signals A to D belong most likely to β-CH$_2$ protons of cysteinyl ligands. Signal E was assigned as a cysteine α-CH proton as its line width is smaller when compared to signals A to D (Figure 2b and Table S2).

Maturation of apo-HydA1 with $[Fe_2(adt)(CO)_4(CN)_2]$ yields HydA1 with a fully functional H-cluster (see Supporting Information SI1). In this [6Fe] system, spin coupling is in effect. For H_{ox} and CO-inhibited H_{ox}–CO state, the H-cluster contains the cubane in the oxidized 2+ state. According to a theoretical model, $[4Fe\text{-}4S]^{2+}_H$ is composed of two valence-delocalized Fe pairs, $[2Fe]_A$ and $[2Fe]_B$, which are antiferromagnetically coupled to each other via the strong intracluster coupling J_{cube} ($\approx$ 200 cm^{-1}).[12] In addition, $[4Fe\text{-}4S]_H^{2+}$ is coupled through $[2Fe]_B$ to $[2Fe]_H$ in the $[Fe_p^{I}Fe_d^{II}]$

DOI: 10.1021/jacs.7b11196
J. Am. Chem. Soc. 2018, 140, 131−134

redox configuration via the intercluster exchange coupling j (Figure 3).

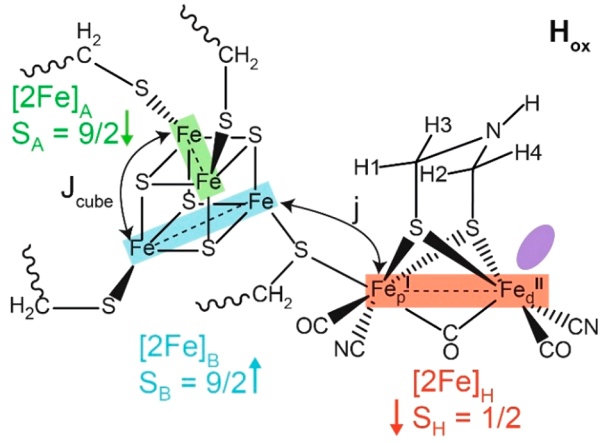

Figure 3. Schematic representation of the active site H-cluster of [FeFe] hydrogenases in the H_{ox} state. The exchange interactions of the H-cluster are indicated. $[4Fe\text{-}4S]_H^{2+}$ is composed of two valence-delocalized Fe(II)−Fe(III) pairs with $S = 9/2$ that are antiferromagnetically coupled by J_{cube}. $[2Fe]_H$ consists of a low-spin Fe(I)−Fe(II) pair with ground state $S = 1/2$, which is coupled via the coupling constant j to $[4Fe\text{-}4S]_H^{2+}$. The violet sphere indicates the open coordination site at Fe_d where substrate or CO bind.

This coupling, previously investigated by ENDOR and Mössbauer spectroscopy, has been found to be about 25 cm^{-1} for H_{ox} and 95 cm^{-1} for H_{ox}−CO.[11,12,22] The 4-fold increased j in the H_{ox}−CO state causes the spin density to be strongly localized on Fe_p, while it is more evenly distributed over Fe_d and Fe_p in the H_{ox} state.[11] Nevertheless, both j values are small compared to J_{cube}. J_{cube} leads to an orientation of S_A antiparallel to S_B and j orients S_H antiparallel to S_B. Hence, S_H is oriented parallel to S_A (Figure 3). Magnitude and sign of the spin density are reflected by the observed proton hyperfine shifts that depend mainly on the Fe−S−C−H dihedral angle θ. The angular dependence of the chemical shift δ follows the general Karplus relationship $\delta = a \cos^2\theta + b \cos\theta + c$ with b and c being small and often neglected.[15] As the remaining angular term $\cos^2\theta$ is always positive, solely the sign of the spin density on the coordinated Fe determines the direction of the paramagnetic shift.

After preparation of HydA1 in the H_{ox} state (see Supporting Information S1 and Figure S4), six downfield shifted resonances are observed in the ^1H NMR spectrum between 11 and 33 ppm and also two upfield shifted resonances at −10 and −21 ppm (Figure 2c). The downfield shifted signals a, b, 1, and 2 exhibit Curie and signals c to f anti-Curie temperature dependence (Table S2 and Figure S2). The two upfield shifted resonances show pseudo-Curie temperature dependence. No hyperfine-shifted signals were detected at positions observed in the spectrum for apo-HydA1. This demonstrates the influence of the $[2Fe]_H$ on the $[4Fe\text{-}4S]_H^{2+}$ cluster via exchange coupling in solution. In order to distinguish the methylene proton resonances originating from the cysteines coordinating $[4Fe\text{-}4S]_H^{2+}$ from those of adt, H_{ox} was also prepared using a deuterated $[2Fe]_H$ site (^{2}H-adt). Thus, the downfield shifted signals 1 and 2 and the upfield shifted signals 3 and 4 (Figures 2c) have been unambiguously assigned to the four methylene protons of $[2Fe]_H$ (Figure S5). They can be attributed to two pairs of geometrically and electronically similar protons. Based on their distances to Fe_p and Fe_d, line widths, and observed ^1H NOE connectivities, signals 1 and 2 are assigned to the axial and signals 3 and 4 to the equatorial protons (Figure 1 and Table S2). Further details are provided in the Supporting Information (SI4, Figure S6 and Table S1).

By flushing active HydA1 with CO, pure H_{ox}−CO state is prepared (see Supporting Information S1 and Figure S7). This CO-inhibited state is an important source of information reporting about the redistribution of spin density in the H-cluster upon binding of an electron donating external ligand to the open coordination site at Fe_d. In its ^1H NMR spectrum, seven downfield and four upfield shifted resonances are observed in the range 11 to 85 ppm and −2 to −30 ppm, respectively (Figure 2d). The downfield shifted signals A, 1, 2, B, C, and D show Curie and E weak anti-Curie temperature dependence. As for the H_{ox} state, all upfield shifted resonances show pseudo Curie temperature dependence (Figure S4). In agreement with an increased j due to coordination of the external CO ligand at Fe_d, ^1H resonances were broader (as much as 4 kHz) and more dispersed than those for all other HydA1 states investigated here (Figure 2 and Table S2). In contrast, the line widths of the contact shifted proton signals of H_{ox} are ∼300 Hz similar to oxidized apo-HydA1. For the H_{ox}−CO state, signals 1 to 4 have been assigned analogous to the H_{ox} state to axial and equatorial protons (Figure S8). Although the temperature dependence of signals 1 to 4 is weak in the H_{ox}−CO state, their temperature-dependence in the H_{ox} state is the strongest of all observed hyperfine shifted resonances in that state (Figures S2 and SI3). This large temperature dependence of the adt methylene protons in the H_{ox} state indicates that the energies of the populated excited states of $[2Fe]_H$ are closer than those of $[4Fe\text{-}4S]_H^{2+}$ and agrees well with j, determined to be small for this state. One possible explanation for the relatively small temperature dependence of the adt methylene protons in the H_{ox}−CO state is that binding of the external CO ligand increases not only j but also the energies of the levels populated at room temperature. The assignment of the methylene protons of the adt bridge provides insight into the spin density at four additional positions of the $[2Fe]_H$ site. Large negative hyperfine shifts are observed for signals 3 and 4 in the H_{ox}, and large positive hyperfine shifts are detected for signals 1 and 2 in the H_{ox}−CO state (Figure 2cd). These hyperfine shifts reflect the larger $[2Fe]_H$ spin density for H_{ox} when compared to H_{ox}−CO, resulting from the different ratio of j and J_{cube}. The NMR spectra observed for the H_{ox} and H_{ox}−CO states can be interpreted based on the spin coupling model described above (Figure 3). Spin-polarization mechanisms will transmit positive and negative spin density to the ^1H atoms of the cysteines coordinating $[2Fe]_A$ and $[2Fe]_B$, respectively. Thus, ligation of $[2Fe]_A$ results in downfield and ligation of $[2Fe]_B$ in upfield shifted ^1H resonances. However, the bridging cysteine experiences not only positive spin density from $[2Fe]_B$ but also negative spin density from $[2Fe]_H$. Taking into account the larger spin density at $[4Fe\text{-}4S]_H^{2+}$ and the lower spin density at $[2Fe]_H$ in the H_{ox}−CO as compared to the H_{ox} state, a net upfield shift is expected for the β-CH_2 protons of the bridging cysteine. Accordingly, peaks F, G, and H can be assigned to the β-CH_2 protons of the bridging and nonbridging cysteine coordinating $[2Fe]_B$ (Figure 2d). For the H_{ox} state, only two upfield shifted resonances are observed because of the smaller spin density at $[4Fe\text{-}4S]_H^{2+}$ resulting from j, which is four-fold smaller than for the H_{ox}−CO state (Figure 2c).

DOI: 10.1021/jacs.7b11196
J. Am. Chem. Soc. 2018, 140, 131−134

We show here that paramagnetic NMR can be applied to the important class of [FeFe] hydrogenases. The derived assignments of the axial and equatorial protons of the unique $[2Fe]_H$ help to reveal intimate details of the different electronic states of the active site required for efficient catalytic H_2 evolution under near-native conditions. Solution NMR titration experiments of HydA1 with its native electron donor PetF[23] are foreseen to provide also experimental insight of HydA1's complex interface as well as dynamics related to complex formation as recently reported for cytochrome P450 and b_5.[24,25] Furthermore, NMR spectroscopy allows for the investigation of HydA1 states with a diamagnetic ground state like H_{red} and $H_{red}H^+$ that are EPR silent. Most importantly, the terminal hydride intermediate, which already has been discussed based on FTIR,[26,27] Mössbauer,[28] and NRVS spectroscopy,[29,30] can be accessed directly at ambient temperatures using solution NMR spectroscopy.

■ ASSOCIATED CONTENT

Supporting Information

The Supporting Information is available free of charge on the ACS Publications website at DOI: 10.1021/jacs.7b11196.

Methods, supplementary NMR and FTIR, and figures and tables (PDF)

■ AUTHOR INFORMATION

Corresponding Authors

*sigrun.rumpel@cec.mpg.de
*wolfgang.lubitz@cec.mpg.de

ORCID

Enrico Ravera: 0000-0001-7708-9208
Claudio Luchinat: 0000-0003-2271-8921
Wolfgang Lubitz: 0000-0001-7059-5327

Notes

The authors declare no competing financial interest.

■ ACKNOWLEDGMENTS

We thank Nina Breuer, Patricia Malkowski, and Inge Heise for sample preparation and synthesis of unlabeled and deuterated $[Fe_2(adt)(CO)_4(CN)_2]$. This work has been supported by iNEXT, grant number 653706, funded by the Horizon 2020 programme of the European Union and COST action FeSBioNet CA15133.

■ REFERENCES

(1) Lubitz, W.; Ogata, H.; Rüdiger, O.; Reijerse, E. *Chem. Rev.* **2014**, *114*, 4081.
(2) Esselborn, J.; Lambertz, C.; Adamska-Venkatesh, A.; Simmons, T.; Berggren, G.; Noth, J.; Siebel, J.; Hemschemeier, A.; Artero, V.; Reijerse, E.; Fontecave, M.; Lubitz, W.; Happe, T. *Nat. Chem. Biol.* **2013**, *9*, 607.
(3) Berggren, G.; Adamska, A.; Lambertz, C.; Simmons, T. R.; Esselborn, J.; Atta, M.; Gambarelli, S.; Mouesca, J. M.; Reijerse, E.; Lubitz, W.; Happe, T.; Artero, V.; Fontecave, M. *Nature* **2013**, *499*, 66.
(4) Adamska, A.; Silakov, A.; Lambertz, C.; Rüdiger, O.; Happe, T.; Reijerse, E.; Lubitz, W. *Angew. Chem., Int. Ed.* **2012**, *51*, 11458.
(5) Adamska-Venkatesh, A.; Krawietz, D.; Siebel, J.; Weber, K.; Happe, T.; Reijerse, E.; Lubitz, W. *J. Am. Chem. Soc.* **2014**, *136*, 11339.
(6) Roseboom, W.; De Lacey, A. L.; Fernandez, V. M.; Hatchikian, E. C.; Albracht, S. P. J. *JBIC, J. Biol. Inorg. Chem.* **2006**, *11*, 102.
(7) Silakov, A.; Wenk, B.; Reijerse, E.; Albracht, S. P. J.; Lubitz, W. *JBIC, J. Biol. Inorg. Chem.* **2009**, *14*, 301.
(8) Silakov, A.; Wenk, B.; Reijerse, E.; Lubitz, W. *Phys. Chem. Chem. Phys.* **2009**, *11*, 6592.
(9) Mulder, D. W.; Ratzloff, M. W.; Shepard, E. M.; Byer, A. S.; Noone, S. M.; Peters, J. W.; Broderick, J. B.; King, P. W. *J. Am. Chem. Soc.* **2013**, *135*, 6921.
(10) Sommer, C.; Adamska-Venkatesh, A.; Pawlak, K.; Birrell, J. A.; Rüdiger, O.; Reijerse, E. J.; Lubitz, W. *J. Am. Chem. Soc.* **2017**, *139*, 1440.
(11) Silakov, A.; Reijerse, E. J.; Albracht, S. P. J.; Hatchikian, E. C.; Lubitz, W. *J. Am. Chem. Soc.* **2007**, *129*, 11447.
(12) Popescu, C. V.; Munck, E. *J. Am. Chem. Soc.* **1999**, *121*, 7877.
(13) Bertini, I.; Luchinat, C.; Parigi, G.; Ravera, E. *NMR of Paramagnetic Molecules*; Elsevier Amsterdam, 2017.
(14) Bertini, I.; Turano, P.; Vila, A. J. *Chem. Rev.* **1993**, *93*, 2833.
(15) Bertini, I.; Capozzi, F.; Luchinat, C.; Piccioli, M.; Vila, A. J. *J. Am. Chem. Soc.* **1994**, *116*, 651.
(16) Lanzilotta, W. N.; Holz, R. C.; Seefeldt, L. C. *Biochemistry* **1995**, *34*, 15646.
(17) Kaufman, J.; Spicer, L. D.; Siegel, L. M. *Biochemistry* **1993**, *32*, 2853.
(18) Bertini, I.; Briganti, F.; Luchinat, C.; Scozzafava, A. *Inorg. Chem.* **1990**, *29*, 1874.
(19) Donaire, A.; Gorst, C. M.; Zhou, Z. H.; Adams, M. W. W.; Lamar, G. N. *J. Am. Chem. Soc.* **1994**, *116*, 6841.
(20) Lebrun, E.; Simenel, C.; Guerlesquin, F.; Delepierre, M. *Magn. Reson. Chem.* **1996**, *34*, 873.
(21) Beinert, H.; Holm, R. H.; Munck, E. *Science* **1997**, *277*, 653.
(22) Silakov, A.; Reijerse, E. J.; Lubitz, W. *Eur. J. Inorg. Chem.* **2011**, *2011*, 1056.
(23) Rumpel, S.; Siebel, J. F.; Diallo, M.; Fares, C.; Reijerse, E. J.; Lubitz, W. *ChemBioChem* **2015**, *16*, 1663.
(24) Ravula, T.; Barnaba, C.; Mahajan, M.; Anantharamaiah, G. M.; Im, S.-C.; Waskell, L.; Ramamoorthy, A. *Chem. Commun.* **2017**, *53*, 12798.
(25) Barnaba, C.; Gentry, K.; Sumangala, N.; Ramamoorthy, A. *F1000Research* **2017**, *6*, 662.
(26) Mulder, D. W.; Ratzloff, M. W.; Bruschi, M.; Greco, C.; Koonce, E.; Peters, J. W.; King, P. W. *J. Am. Chem. Soc.* **2014**, *136*, 15394.
(27) Winkler, M.; Senger, M.; Duan, J. F.; Esselborn, J.; Wittkamp, F.; Hofmann, E.; Apfel, U. P.; Stripp, S. T.; Happe, T. *Nat. Commun.* **2017**, *8*, 16115.
(28) Mulder, D. W.; Guo, Y. S.; Ratzloff, M. W.; King, P. W. *J. Am. Chem. Soc.* **2017**, *139*, 83.
(29) Reijerse, E. J.; Pham, C. C.; Pelmenschikov, V.; Gilbert-Wilson, R.; Adamska-Venkatesh, A.; Siebel, J. F.; Gee, L. B.; Yoda, Y.; Tamasaku, K.; Lubitz, W.; Rauchfuss, T. B.; Cramer, S. P. *J. Am. Chem. Soc.* **2017**, *139*, 4306.
(30) Pelmenschikov, V.; Birrell, J. A.; Pham, C. C.; Mishra, N.; Wang, H.; Sommer, C.; Reijerse, E.; Richers, C. P.; Tamasaku, K.; Yoda, Y.; Rauchfuss, T. B.; Lubitz, W.; Cramer, S. P. *J. Am. Chem. Soc.* **2017**, *139*, 16894.

■ NOTE ADDED AFTER ASAP PUBLICATION

This paper was published on December 14, 2017. The abstract has been corrected and the revised version was re-posted on December 19, 2017.

DOI: 10.1021/jacs.7b11196
J. Am. Chem. Soc. 2018, 140, 131−134